EA

DESIGN CRITERIA FOR RECTANGULAR SUPERCONDUCTING COILS FOR TRANSPORT APPLICATIONS

E. Abel, J.P. Howell, J.L. Mahtani, R.G. Rhodes

Paper presented at the 6th INTERNATIONAL CONFERENCE ON MAGNET TECHNOLOGY, BRATISLAVA 29 August - 2 September 1977

pp. 163 - 171

Abstract

Design criteria are established for finite radius rectangular superconducting coils as designed for magnetically levitated trains. Two approaches are followed. A simple stress analysis of a finite radius rectangular coil is presented which compares the stress level in the coil with an equivalent circular coil, for which anistropy can be included. The limiting radius for a particular stress level can hence be chosen.

Using the impedance modelling technique establishes the degradation of lift to drag ratio and dependence of lateral stiffness on the variation of corner radius for the Warwick Maglev Geometry.

1. Introduction

The use of superconducting magnets for both the levitation and linear motor propulsion of high speed trains is being considered by different groups in several countries[1]. The majority of designs are based on rectangular or square coils, which will be wound as racetrack coils - i.e. with semicircular end windings. This arrangement relieves the manufacturing and operational difficulties associated with sharp corners, of winding migration and stress concentration. However, for the coordinated maglev system combining levitation, guidance and propulsion being studied at the University of Warwick, the magnetic forces are generated by all four sides of a magnet in a longitudinal array of magnets on the vehicle. Any deviation from a rectangular magnet results in a degradation of the required magnetic forces.

Proposed maglev systems tend to choose long thin levitation magnets to produce enhanced lift to drag ratios. For example the Canadian Reference Design[2] comprises eight 1.0 m x 0.3 m levitation magnets, for a 30 tonne vehicle. The propulsion magnets' size is determined by thrust requirements, passenger density and hardware costs, but generally a wavelength in the range 1-3 meters seems reasonable[3]. The vehicle width naturally constrains the space left for a propulsion magnet array, after levitation magnets are sized. For a full racetrack end-wound propulsion coil, linear motor active length is reduced by about half a wavelength, compared to a rectangular coil. If a transverse-flux or dual-motor configuration[4] is adopted, then four sets of machine magnet endwindings have to be accommodated in the vehicle width.

In this paper, a simplified method for stressing finite radius rectangular coils, based on comparison with a circular solenoid equivalent is presented, and model measurements illustrate the effects of transition from a square to a circular geometry on lift to drag ratio and guidance stiffness for the Warwick flat track maglev system.

2. Stress Analysis

2.1 Previous Analysis

Many authors have established methods of analysis of varying complexity to determine the forces on coil systems. Essentially the forces can be put into three categories[5].

1) Mechanical, due to coil winding, pre-stressing and support.
2) Thermomechanical forces due to uneven material contraction during cool-down.
3) Magnetomechanical forces when the coil is energized.

The stresses arising from category (3) forces are those discussed in this paper.

In the case of a circular superconducting solenoid, the stress levels can be easily computed using a thick/thin cylinder approximation[6]. A homogeneous thick cylinder theory produces a more accurate solution[7]. Since the coils are anisotropic structures, account must be taken of the orthotropy, in evaluating the stress tensor. Mulhall analyzes a homogeneous anistropic solenoid[8], and several more recent papers consider transversely isotropic solenoids[9] and stresses in anistropic coils[10,11] under the three force categories previously mentioned.

2.2 Simplified Analysis

For a coil structure with a finite corner radius it can be assumed that the most critical stress levels will be reached at the corners. In place of the exact solution that was possible with circular coils, several approximate solutions can be formulated and referenced to a circular coil stress level.

In particular the analysis is based on a magnetic pressure comparison of rectangular and square tubes with a circular thick walled tube, since the free-body diagram of sections of the two cases are identical. When a circular coil is analysed, an exact solution approaches that derived by a magnetic pressure approximation if the coil build is small compared to its diameter[12]. This condition is usually met by maglev coils, where the strength is of the order of 500 kAT. for the motor magnets, and size is of the order of 0.5-3 m x 1-3 m.

2.2.1 - Circular Coil

The case of a circular coil of mean radius a, winding width c and magnetic pressure P_m produces hoop stress σ_θ, radial stress σ_r and shear stress σ_s given by:

$$\sigma_\theta = P_m \cdot \frac{\left(a^2 + \frac{c^2}{4}\right)}{ac} = \frac{1 + \left(\frac{2a}{c}\right)^2}{4\left(\frac{a}{c}\right)} P_m \quad N/m^2 \qquad (1)$$

$$\sigma_r = -P_m \quad N/m^2 \qquad (2)$$

$$\sigma_s = \frac{\sigma_\theta - \sigma_r}{2} = \frac{\left(1 + \left(\frac{2a}{c}\right)^2\right)}{8\left(\frac{a}{c}\right)} P_m \quad N/m^2 \qquad (3)$$

These values are for the inside face of the wound section, where the shear stress is a maximum.

2.2.2 Magnetic Pressure

The magnetic pressure, P_m is taken as identical to the coil energy density,

$$\text{i.e.} \quad P_m = \frac{1}{2\mu_0} B^2 \quad J/m^3, \text{ or } N/m^2 \qquad (4)$$

where B is the coil flux density.

Naturally the coil flux density is modified for the same ampere turns as the corner radius is changed. The central field normalized by the factor $\frac{\mu_o I}{\pi a}$ is plotted in Figure 1 for the transition from a square coil to a circular coil. The values range from $\frac{\pi}{2}$ for a circular coil to $\sqrt{2}$ for a square coil. Although the value of flux density to be used in equation (4) should be that of the inner face of the coil, the central field value from Figure 1 is a reasonable guide to the exact value.

2.3 Rectangular frame or tube under uniform outward pressure

Figure 2a,b shows the simple portal frame or square edged tube of meanside 2a and $2\gamma a$. Roark[13] gives values of the corner moment,

$$M = \frac{1}{12} . w . (2a)^2 . \left(\frac{1 + \gamma^3}{1 + \gamma}\right) \qquad (5)$$

where w is the uniform loading, related to the internal pressure P_m by

$$w = d . P_m \qquad (6)$$

where d is the depth of the finite section.

For the case of a square coil, $\gamma = 1$ and eqtn. (5) reduces to

$$M = \frac{wa^2}{3} \qquad (7)$$

The maximum stress is at the inner edge, so

$$\sigma_\theta = \frac{M . c/2}{I} = 2 \frac{a^2}{c^2} P_m \qquad (8)$$

2.4 Rectangular tube with radiused corners under uniform outward pressure

Figure 2c,d shows a radiused corner tube, again under pressure P_m. The maximum bending moment occurs at the corner and is given by

$$M = Cw (2\gamma a)^2 \qquad (9)$$

where C is shown in Figure 3, the values obtained from Reference 12, for $\gamma = 1$.

The fibre stress is given as before, by

$$\sigma_\theta = \frac{M \frac{c}{2}}{I} = 24 \frac{a^2}{c^2} C P_m \qquad (10)$$

Note that if $\frac{r}{a} = 0$ (square coil), $C = \frac{1}{12}$ and equation (10) reverts to equation (8)

The stress given by equation (10) needs further modification to take into account the deviation of the neutral axis from the centroidal axis.

The actual stress at the innermost fibre is given by

$$\sigma_\theta = k_i \, (\sigma_\theta \text{, equation 10}) \tag{11}$$

$$\text{where } k_i = 1 + \frac{c}{6r} \left(\frac{1}{1 - \frac{c}{2r}} + 1 \right) \tag{12}$$

and so

$$\sigma_\theta = 24 \left(\frac{a}{c}\right)^2 C \, k_i \, P_m$$

$$\sigma_\theta = 24 \left(\frac{a}{c}\right)^2 C \left[1 + \left(\frac{c}{6r}\right) \left(\frac{1}{1 - \frac{c}{2r}} + 1 \right) \right] P_m \tag{13}$$

As in section 2.2.1,

$$\sigma_r = - P_m \tag{14}$$

$$\text{and} \quad \sigma_s = \frac{\sigma_\theta - \sigma_r}{2} \tag{15}$$

Using equations (13) and (15), the radius for a particular wound section (implying c and d) can be found where the stress level equals that of an equivalent circular coil of the same section. The circular equivalent coil can then be analysed using exact solutions and including anistropy.

3 Impedance Modelling

3.1 Technique

The magnetic forces generated by a maglev vehicle can be analysed using the impedance modelling technique[14]. Previous work[15] has suggested that at high speeds the lift and drag forces of a square coil are identical to those obtained from a circular coil. This applied to an infinite sheet conductor and to assess the influence of a split track a series of coils were wound with different corner radii (Figure 4).

The two parameters of interest are the lift to drag (L/D) ratio, which is a measure of the power requirement, and the guidance stiffness Y_y', which defines the stability. The guidance stiffness Y_y' is given by

$$Y_y' = \frac{\partial Y/\partial y}{2\ mga} \qquad (16)$$

where 2a is the coil width, Y is the lateral restoring force, y is the lateral displacement, mg is the vehicle weight (i.e. the lift force at the equilibrium position).

3.2 Results

Using a single coil over a split track, the L/D ratio and Y_y' have been measured for a range of track conductor spacings. The results are shown in Figures 5 and 6. The data has been scaled to give the forces on a 1.6 m long coil, moving at 135 m/s, with a clearance of 0.24 m over an aluminium track 10 mm thick. Each conductor is assumed to be 0.75 m wide. The results have been normalised to the square coil value obtained when the coil overlaps each conductor by 40 mm full scale $(\frac{2}{z}(a - a') = 0.33)$. In this position two coils in tandem and of opposite polarity generate a L/D ratio of 25, and have a guidance stiffness of Y_y' of 6.4, which is sufficient to give a lateral oscillation frequency of 1 Hz[16].

It is apparent that the optimum coil-track geometry occurs at different track spacings for each shape. The L/D ratio as a function of corner radius is plotted in Figure 7 for two values of guidance stiffness, corresponding to lateral oscillation frequencies of 1 Hz and 1.4 Hz. In both cases the circular coil shows a reduction in lift to drag ratio of 27% when compared with the square coil.

3.3 Effect on Power Requirement

If a magnet array of circular coils is used instead of square coils, the magnet drag power is increased by 37%. However the dominating drag force for maglev vehicles arises from aerodynamic effects. For example a vehicle moving at 135 m/s has to overcome an aerodynamic drag force of approximately 3 tonnes[17]. ($C_x = 0.3$, $9m^2$ frontal area). For a 30 tonne vehicle the magnetic drag force is 1.2 tonnes if the suspension magnets are square coils (L/D = 25). The total power requirement in changing from square to circular coils is therefore increased by only 10%.

Conversely, if the track thickness is increased by 37% then the circular coil requires the same power input as the square coil. In comparison with other track designs[16], the Warwick design would still be the most economical in terms of guideway aluminium costs.

4. Conclusions

The two main areas of interest in determining the choice of magnet endwinding shape for cryogenic maglev are

1) Magnitude of self forces in coils
2) Effects on electrodynamic system performance

A simple method has been presented to enable first estimates to be made on stress levels in rectangular coils with corner radii. Comparison with circular coils under the same magnetic pressure establishes the allowable size of corner radius.

The effects on the lift to drag ratio and guidance stiffness as corner radius changes is qualified for the proposed Warwick geometry. A reduction in performance must be accepted with increasing corner radius.

The paper presents only the first steps in an analysis of a system. Further work is necessary in detail for each component of the system before full specification can be achieved.

5. References

1. Maglev Issue, Cryogenics, Vol. 15 No. 7, July 1975, p.371-405.

2. Canadian Institute of Guided Ground Transport 'Superconducting Linear Synchronous Motor Propulsion and Magnetic Levitation for High Speed Guided Ground Transportation' CIGGT Report 76-7, March 1976.

3. E. Abel et al, 'An Assessment of Linear Superconducting Motors for Maglev', IEE Conference Publication No. 142, p. 125-7, 2nd Conference on Advances in Magnetic Materials and their Applications.

4. P.E. Burke et al 'A Dual Linear Synchronous Motor for Maglev Vehicles', IEEE Trans. Vol. MAG-13, No. 5, September 1977, p. 1415-7.

5. H. Brechna 'Superconducting Magnet Systems', Springer-Verlag, Berlin, 1973.

6. A.D. Appleton et al "Some Design Aspects of a Large Superconducting Magnet", Proc. 2nd International Conference on Magnet Technology, Oxford 1967, p. 553-9.

7. A.J. Middleton, C.W. Trowbridge 'Mechanical Stresses in Large High Field Magnet Coils', ibid, p.140-9.

8. B.E. Mulhall, D.H. Prothero, 'Mechanical Stresses in Solenoid Coils' J.Phys.D., Vol. 6, 1973, p.1973-7.

9. W.H. Gray, J.K. Ballou, 'Electromechanical Stress Analysis of Transversely Isotropic Solenoids', J.Appl.Phys. Vol. 48. No. 7, July 1977, p.3100-9.

10. V. Arp, 'Stresses in Superconducting Solenoids', ibid, Vol. 48, No. 5, May 1977, p. 2026-36.

11. J. Kokavec, L. Cesnak, 'Mechanical Stresses in Cylindrical Superconducting Coils', J.Phys.D., Vol. 10, August 1977, p.1451-9.

12. D.B. Montgomery, 'Solenoid Magnet Design', Wiley, New York 1969.

13. R.J. Roark 'Formulas for Stress and Strain' McGraw Hill, New York, 1965.

14. J.Y. Wong et al 'Impedance Modelling Technique for Investigating the Characteristics of Electrodynamic Levitation Systems', J.Phys.D., Vol. 8, 1975, p.1948-55.

15. Canadian Maglev Group 'Study of Magnetic Levitation and Linear Synchronous Motor Propulsion', December 1972. CIGGT Report 73-1.

16. J.P. Howell et al 'Electrodynamic Levitation of High Speed Vehicles', 2nd Conference on Advances in Magnetic Materials and their Applications, 1-3 September 1976, IEE Conference Publication No. 142, p.117-20.

17. J.P. Howell 'Aerodynamic Lift Characteristics of a Maglev Vehicle' N.P.L. Industrial Aerodynamic Meeting, 23 February 1975, (unpublished).

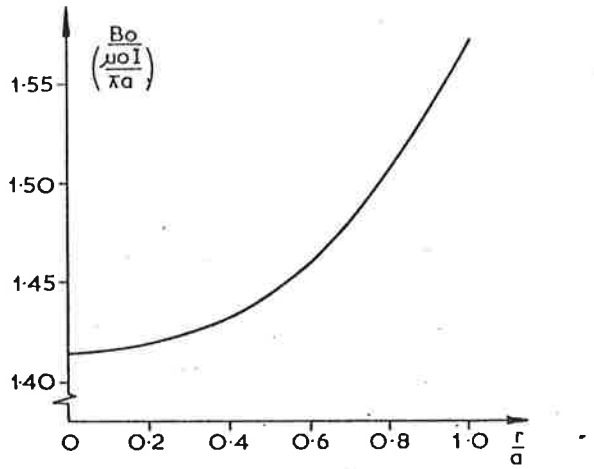

Figure 1. Variation of central field with corner radius.

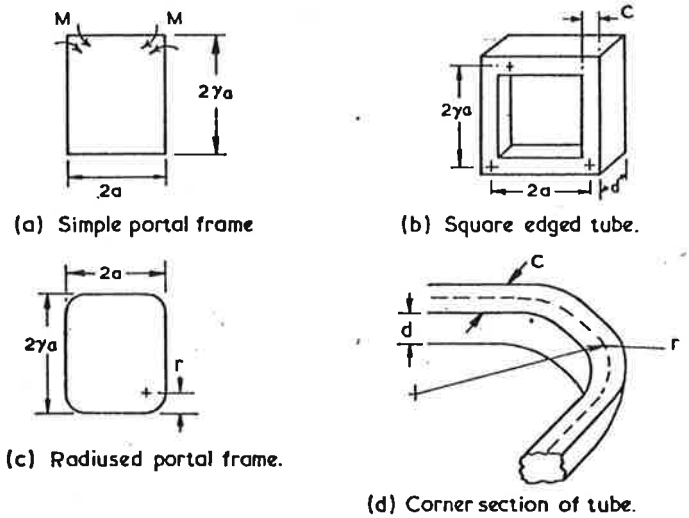

Figure 2. Tube equivalents to radiused coils

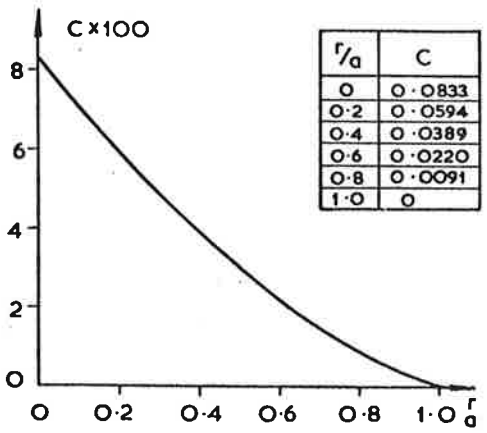

r/a	C
0	0·0833
0·2	0·0594
0·4	0·0389
0·6	0·0220
0·8	0·0091
1·0	0

Figure 3 Variation of C with r/a.

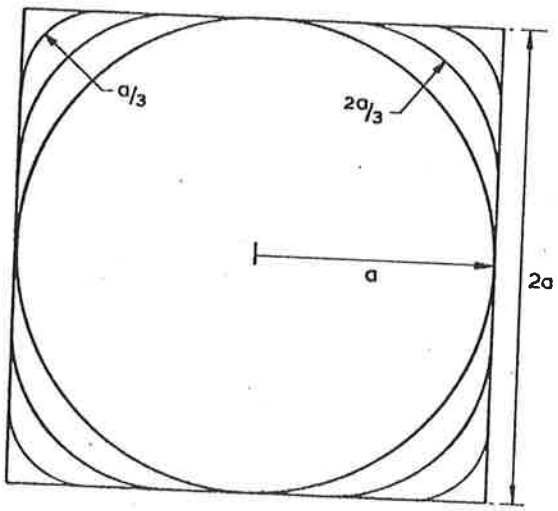

Figure 4. Coil geometries Scale 3/10

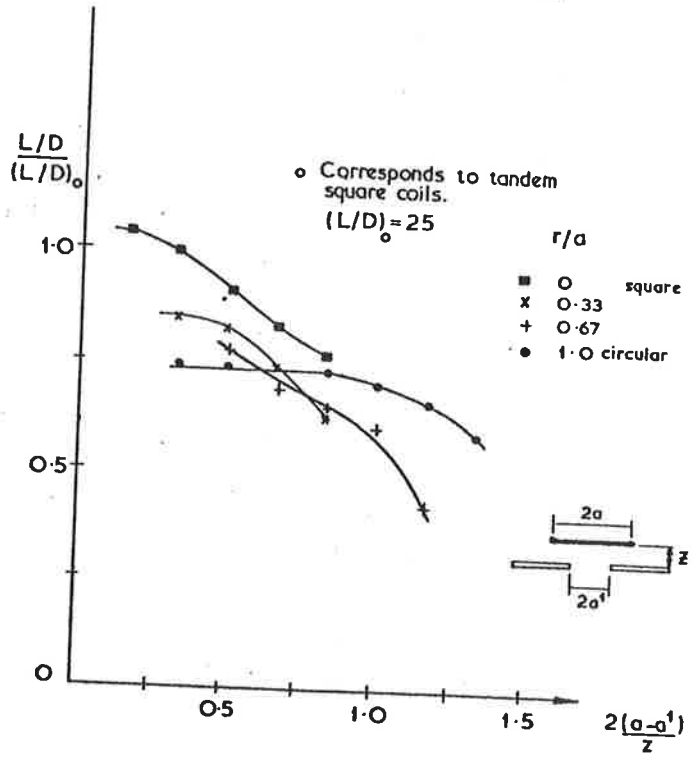

Figure 5. Lift to drag ratio.

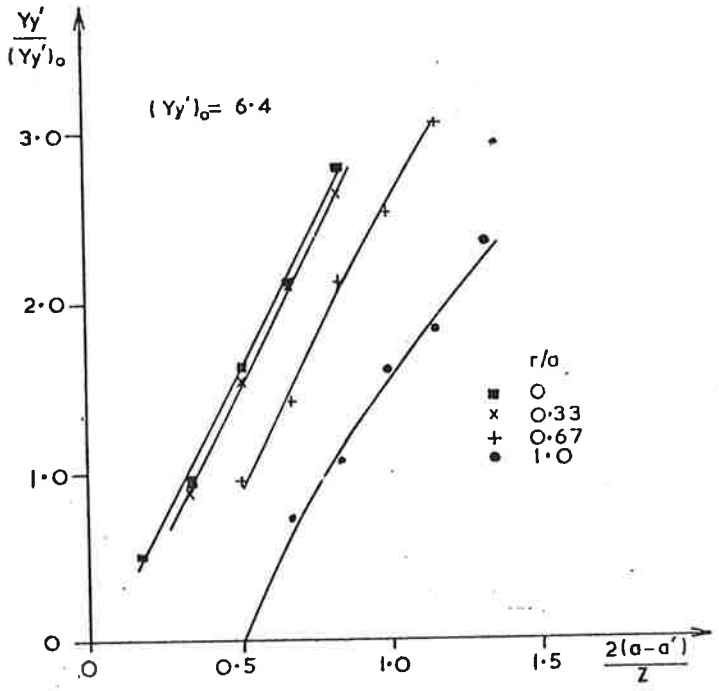

Figure 6 Guidance Stiffness

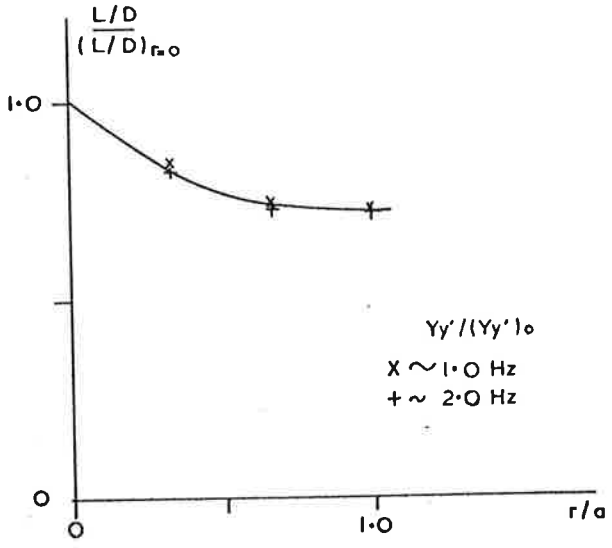

Figure 7 L/D at constant guidance

DISCUSSION

C.P. Parsch : What is the expected levitation weight and the lift force of the described magnets?

R.G. Rhodes : The lift force is equal to the vehicle weight /150 kg/ at a coil centre - track clearance of 100 mm.

P. Komarek : Which are the major advantages of your levitation system in comparison to that investigated elsewhere, e.g. in Japan and in FRG?

R.G. Rhodes : The main advantages are : i - the conceptual simplicity, possibly leading to cheaper and more reliable magnets, ii - the track aluminium requirements are 1/2 to 1/3 those of other systems.

P. Komarek : What are the limits in guidance force?

R.G. Rhodes : The track can be designed to give guidance forces equal to the vehicle weight.

B. Ingram : Had they considered the use of Finite Element Methods of determining the bending stresses in the coils in the presence of side supports?

R.G. Rhodes : No, as the stress levels in our small coils are not large enough to require accurate analysis.